Available online at www.sciencedirect.com
ScienceDirect
Journal of Power Sources 177 (2008) 457–463
JOURNAL OF POWER SOURCES
www.elsevier.com/locate/jpowsour

Short communication

Effect of PTFE content in microporous layer on water management in PEM fuel cells

Sehkyu Park, Jong-Won Lee, Branko N. Popov *

Center for Electrochemical Engineering, Department of Chemical Engineering, University of South Carolina, Columbia, SC 29208, USA

Received 27 August 2007; received in revised form 19 November 2007; accepted 20 November 2007
Available online 23 November 2007

Abstract

The effect of hydrophobic agent (PTFE) concentration in the microporous layer on the PEM fuel cell performance was investigated using mercury porosimetry, water permeation experiment, and electrochemical polarization technique. The mercury porosimetry and water permeation experiments indicated that PTFE increases the resistance of the water flow through the GDL due to a decrease of the MPL porosity and an increase of the volume fraction of hydrophobic pores. When air was used as an oxidant, a maximum fuel cell performance was obtained for a PTFE loading of 20 wt.%. The experimental polarization curves were quantitatively analyzed to determine the polarization resistances resulting from different physical and electrochemical processes in the PEM fuel cell. The polarization analysis indicated that the optimized PTFE content results in an effective water management (i.e., a balancing of water saturations in the catalyst layer and the gas diffusion layer), thereby improving the oxygen diffusion kinetics in the membrane-electrode assembly.
Published by Elsevier B.V.

Keywords: Proton exchange membrane fuel cell; Gas diffusion layer; Microporous layer; Hydrophobic agent; Water management

1. Introduction

Proton exchange membrane (PEM) fuel cells for automotive applications should be able to operate in a wide current range, even at limiting currents, in order to meet high power requirements [1]. Various approaches have been developed to achieve high limiting current densities of PEM fuel cells by tailoring the membrane-electrode assembly (MEA) structure. One of the most effective approaches is to use a gas diffusion layer (GDL) with a dual-layer structure—(i) a carbon-fiber cloth or paper substrate that serves as a current collector and as a physical support for the electrode, and (ii) a thinner microporous layer (MPL) that consists of carbon black powder and a hydrophobic agent, usually polytetrafluoroethylene (PTFE) [2–22]. The MPL reduces a contact resistance between the catalyst layer and the macroporous carbon substrate by forming a flat and uniform layer that is not permeable to the catalyst particles. More importantly, it has been widely reported that the MPL improves water management in the MEA and hence the overall fuel cell performance.

From a simulation study based on the water vapor condensation kinetics and the capillary motion of the condensate, Nam and Kaviany [14] showed that the MPL reduces liquid water saturation at the interfaces between the MPL and the macroporous carbon substrate and between the catalyst layer and the MPL, thus impeding severe water flooding. Similarly, Weber et al. [15] developed an analytical model to examine the effect of wettability of the diffusion media on water management, and demonstrated that owing to its higher hydrophobicity and lower porosity the MPL is less susceptible to water flooding than the carbon substrate and hence leads to a decreased liquid saturation in the cathode compartment during fuel cell operation.

Extensive work has been performed to examine how the MPL properties such as (i) carbon powder type, (ii) carbon loading (or thickness), and (iii) PTFE content control the water management in PEM fuel cells. Passalacqua et al. [6] showed that the MPL prepared with Shawinigan acetylene black led to a better fuel cell performance when compared to the MPLs made using Asbury graphite 850, Mogul L and Vulcan XC-72. The observed

* Corresponding author. Tel.: +1 803 777 7314; fax: +1 803 777 8265.
E-mail address: popov@engr.sc.edu (B.N. Popov).

0378-7753/$ – see front matter. Published by Elsevier B.V.
doi:10.1016/j.jpowsour.2007.11.055

performance improvement was attributed to higher pore volume and smaller pore size of acetylene black, reducing the amount of water accumulated inside the MPL. In our previous study [13], the effect of carbon loading in the MPL on the fuel cell performance was investigated. We proved experimentally that carbon loading of 0.5 mg cm^{-2} under a specific operating condition used in the study results in a maximum liming current density. The ac-impedance study indicated that the optimized carbon loading adjusts water saturations in the catalyst layer and the GDL effectively, resulting in better oxygen transport at the cathode.

The PTFE serves as a binder to maintain the integrity of carbon particles in the MPL, and provides high hydrophobicity to avoid water flooding. The optimized value of PTFE content reported in literature [3–5,7] varies widely from 10 to 30 wt.%, depending on the MEA structure and the fuel cell operating condition. For example, Giorgi et al. [4] reported the best fuel cell performance using the MPLs loaded with 10 wt.% PTFE at ambient pressure, whereas Lufrano et al. [5] showed that the optimum PTFE loading was around 20 wt.% in a pressurized system.

Pasaogullari and co-workers [16,17] simulated two-phase transport in a dual-layer GDL using the multi-phase mixture formulation, and examined specifically the effect of the hydrophobic MPL contact angle on water management. They showed that liquid water saturation at the catalyst layer/MPL interface and within the GDL decreases exponentially with increasing the MPL contact angle (i.e., increasing the MPL hydrophobicity), but it remains nearly constant beyond a certain value of the contact angle (e.g., ca. 105° in their simulation). Weber and Newman [18] have performed a rigorous simulation analysis of water management in PEM fuel cells, and their simulation analysis indicated that a high volume fraction ($\geq$0.8) of hydrophobic pores introduced by PTFE minimizes water flooding in the MEA. However, few experimental studies have been completed to understand the specific role of PTFE (in the MPL) in controlling liquid water saturation that determines the limiting current density of the PEM fuel cell.

The objective of the present work is to study the effect of PTFE content in the MPL on water management in PEM fuel cells. The MPLs were prepared with different PTFE amounts on the macroporous carbon-fiber substrate. Water permeation experiment was performed to characterize the resistance to liquid water flow through the GDL. Electrochemical polarization curves of PEM fuel cells were quantitatively analyzed to discuss oxygen transport limitations (concentration polarization) in the catalyst layer and the GDL as a function of PTFE loading in the MPL.

2. Experimental

2.1. Preparation of microporous layer on the carbon-fiber substrate

The carbon slurry for the MPL was prepared using the following procedure: The carbon powder (acetylene black) was mixed with PTFE-dispersed water (60 wt.% PTFE, Alfa Aesar), isopropyl alcohol and glycerol in an ultrasonic bath for 2 h. The resulting carbon slurry was coated onto one side of the macroporous carbon substrate using a doctor-blade technique, and pressed with two rotating drums at 80 °C to make the MPL uniform and compact. The macroporous substrate used was a carbon-fiber paper pre-treated with 10 wt.% PTFE (SGL 10CA, SGL Carbon Group). The GDL sample was heat-treated at 280 °C for 30 min to evaporate all remaining glycerol, and then at 350 °C for 30 min to uniformly distribute PTFE throughout the MPL. In the MPL, the carbon loading was maintained at 2.0 mg cm^{-2}, and the PTFE content was varied between 10 and 40 wt.%.

2.2. Physical characterizations of the gas diffusion layer

Porous structure of the GDL was characterized by using a mercury porosimeter (Micrometrics Autopore 9500). Cumulative pore volume was determined from the mercury intrusion data, i.e., the volume of mercury penetrating into the pores versus the applied pressure. Under the assumption that all pores are cylindrical, the pore diameter d_p was calculated from the value of the applied pressure using a capillary law [23].

The water permeation characteristics through the GDL were determined using a membrane filtration cell, as proposed by Benziger et al. [24]. The GDL sample with a diameter of 3 cm was placed into the membrane filtration cell. Water was slowly added to the cylinder in the cell until water started to flow through the GDL. The hydrostatic head (i.e., water level in the cylinder) was converted to the pressure, and the threshold pressure p_{th} was defined as the hydrostatic pressure value at which water starts to flow through the GDL. The water permeation measurement was performed at 25–75 °C.

2.3. Preparation of membrane-electrode assembly

The cathode catalyst ink was prepared by ultrasonically blending Pt/C powder (45 wt.% Pt, Tanaka) with Nafion^{TM} solution (5 wt.% Nafion^{TM}, Alfa Aesar), deionized water and methyl alcohol for 2 h. The catalyst ink was sprayed onto one side of Nafion^{TM} 112 membrane, followed by drying at 80 °C for 2 min. The process was repeated until a total Pt loading of 0.4 mg cm^{-2} has been achieved. A commercially available catalyzed GDL (20 wt.% Pt/C, 0.4 mg cm^{-2} Pt, E-TEK) was used as the anode for all fuel cell tests. A thin layer of Nafion^{TM} (1.2 mg cm^{-2}) was coated on the anode surface to improve the adhesion between the catalyst layer and the membrane. The Nafion^{TM}-coated anode was hot-pressed to the uncatalyzed side of the membrane at 140 °C and at 15 atm for 90 s. Finally, the GDL of interest was placed on the cathode catalyst layer.

2.4. Electrochemical polarization experiments

The electrochemical experiments were carried out in a single cell with serpentine flow channels. Pure hydrogen gas humidified at 77 °C and air (or oxygen) humidified at 75 °C were supplied to the anode and cathode compartments, respectively. All measurements were performed at 75 °C and at ambient pres-

sure. Polarization measurements were conducted with a fully automated test station (Fuel Cell Technologies Inc.) under the constant stoichiometry mode using a 30 mV potential step and a 2 min dwell time. The stoichiometries of hydrogen λ_{H_2}, oxygen λ_{O_2}, and air λ_{air} were 1.5, 2.0, and 2.0, respectively. The geometric area of the MEA used in this study was 25 cm^2.

3. Results and discussion

Fig. 1 shows the cumulative pore volumes in the GDLs measured for different PTFE contents in the MPLs. The pore diameters and the pore volumes were estimated from the analyses of mercury intrusion data. The average pore diameter $d_{p,avg}$ was given in Fig. 1. As shown in Fig. 1, the cumulative pore volume in the pore size range of 0.01 and 30 μm decreases with increasing the PTFE content in the MPL, which indicates that PTFE reduces the MPL porosity.

Fig. 2 illustrates the plots of the threshold pressure p_{th} for liquid water flow against the PTFE loading in the MPL, measured from the water permeation experiments. As the PTFE content increases from 10 to 40 wt.%, the value of p_{th} increases from 1.8 to 3.5 kPa. This implies that it is necessary to apply a higher pressure to force the liquid water to penetrate through the GDL in case of higher PTFE loading in the MPL. An increase in water flow resistance with the PTFE loading is attributed not only to an increased volume fraction of hydrophobic pores in the MPL, but also to a decreased MPL porosity as shown in Fig. 1. The water permeation measurements were also conducted using the MPL loaded with 20 wt.% PTFE at different temperatures of 25–75 °C, as presented in Fig. 2. The decreasing tendency of p_{th} with increasing temperature at a given PTFE content is due to the reduced surface tension γ and contact angle of liquid water with pore surface θ at higher temperatures [23].

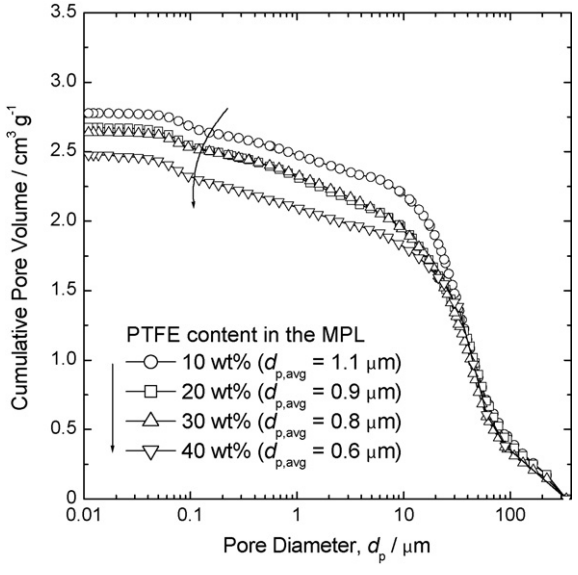

Fig. 1. Cumulative pore volumes in the GDLs measured for different PTFE contents in the MPLs. The pore diameters and the pore volumes were determined from the mercury intrusion data.

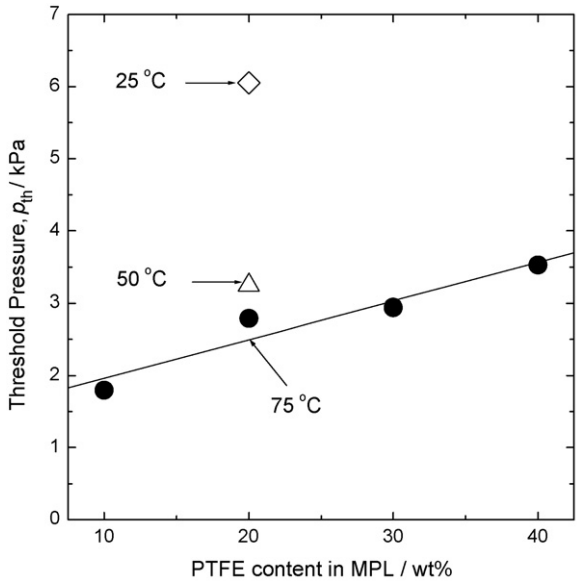

Fig. 2. Plots of the threshold pressure p_{th} for liquid water flow as a function of PTFE loading in the MPL, measured from the water permeation experiments at 75 °C. The data obtained at 25 and 50 °C were also presented for 20 wt.% PTFE in the figure.

Under the assumption that the pores are cylindrical and the value of θ is constant ($\theta = 108°$) [16,25], the effective pore diameter $d_{p,eff}$ for liquid water penetration at 75 °C was calculated from the value of threshold pressure, p_{th} using the Young–Laplace equation:

$$d_{p,eff} = \frac{4\gamma \cos\theta}{p_{th}} \quad (1)$$

The result summarized in Table 1 indicates that the size of pores involved in water flow becomes smaller for higher PTFE content in the MPL.

Fig. 3(a) shows polarization curves of the PEM fuel cells measured using the MPLs with different PTFE loadings. The experiments were performed with H_2 and air under the constant stoichiometry mode of $\lambda_{H_2} = 1.5$ and $\lambda_{air} = 2.0$. The fuel cell performance reaches a maximum for 20 wt.% PTFE, and then decreases with further increasing the PTFE content in the MPL. This means that there exist optimum hydrophobicity and MPL porosity for effective transport of gaseous oxygen and liquid water inside the MEA.

The experimental polarization curves in Fig. 3(a) were quantitatively analyzed to determine the polarizations resulting from different physical and electrochemical processes in the PEM fuel cell using the procedure proposed by Williams et al. [26]. It was

Table 1
Effective pore diameter $d_{p,eff}$ for liquid water flow through the GDL calculated from the threshold pressure p_{th}

PTFE content in the MPL (wt.%)	$d_{p,eff}$ at 75 °C (μm)
10	43.8
20	28.1
30	26.7
40	22.3

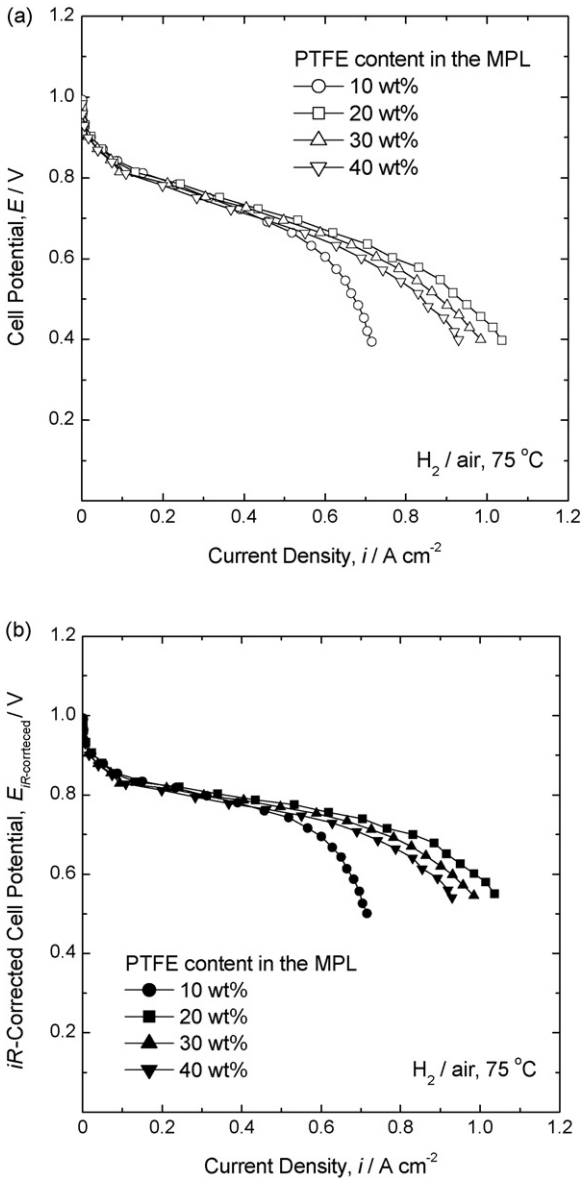

Fig. 3. (a) Polarization curves of the PEM fuel cells measured using the MPLs with different PTFE loadings. The measurements were performed at 75 °C using H_2 and air under the constant stoichiometry mode of $\lambda_{H_2} = 1.5$ and $\lambda_{air} = 2.0$. (b) Polarization curves corrected for the total ohmic losses (i.e., iR, where $R = R_1 + R_2$).

assumed that the oxygen reduction kinetics at the three-phase boundary follows the Butler–Volmer equation that is first order in oxygen concentration, and the overpotential of anode compartment is negligibly small. The latter assumption is valid, since the exchange current density for hydrogen oxidation is higher by several orders of magnitudes than that for oxygen reduction, and pure hydrogen gas was supplied to the anode. Under these assumptions, the following overpotentials contribute to the total overpotential measured experimentally: (i) ohmic loss due to an internal resistance (R_1) of the membrane, GDL and other cell components (e.g., flow field, current collector, etc.), (ii) ohmic loss due to an internal resistance (R_2) of the cathode catalyst layer, (iii) oxygen concentration polarization in the cathode GDL, (iv) oxygen concentration polarization in the cathode catalyst layer, and (v) activation polarization associated with oxygen reduction kinetics at the three-phase boundaries among Pt catalyst, ionomer and gas. In this work, the main focus was on the concentration polarizations in the cathode GDL and the cathode catalyst layer to understand how PTFE in the MPL controls liquid water saturation and oxygen transport in both layers.

Table 2
Internal ohmic resistance of the membrane, GDL and other cell components, R_1, and the internal ohmic resistance of the cathode catalyst layer, R_2

PTFE content in the MPL (wt.%)	R_1 (mΩ cm^2)	R_2 (mΩ cm^2)
10	92.6	57.2
20	92.8	55.1
30	93.2	56.1
40	93.6	60.0

The measured cell potential E in Fig. 3(a) was compensated for ohmic losses (iR_1 drop) of the membrane, GDL and other cell components using a current-interruption technique. It is generally known that the ohmic potential drop resulting from R_1 occurs with in a few micro- or milliseconds. Because of a relatively slow relaxation process in the catalyst layer, the iR_1-corrected cell potential, $E_{iR_1\text{-corrected}}$, was further corrected for ohmic losses (iR_2 drop) of the cathode catalyst layer as follows [26]: the ratio of O_2 concentration in pure oxygen gas to that in air is approximately 4.8. This means that if the iR_2 drop were negligible, the current density i_{O_2} measured with pure oxygen would be 4.8 times the current density i_{air} measured with air under the assumption that oxygen reduction kinetics is first order in oxygen concentration.

In this study, however, the comparison of the experimental $i - E_{iR_1\text{-corrected}}$ curves measured with oxygen and air indicated that the ratio of i_{O_2} to i_{air} at a given $E_{iR_1\text{-corrected}}$ was lower

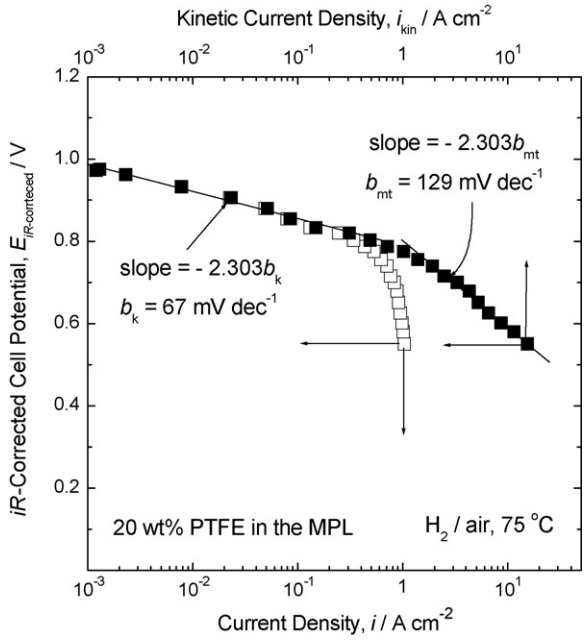

Fig. 4. iR-corrected polarization curves of the PEM fuel cells presented in terms of the measured current density i and the kinetic current density i_{kin} (Eq. (2)). The PTFE content in the MPL was 20 wt.%.

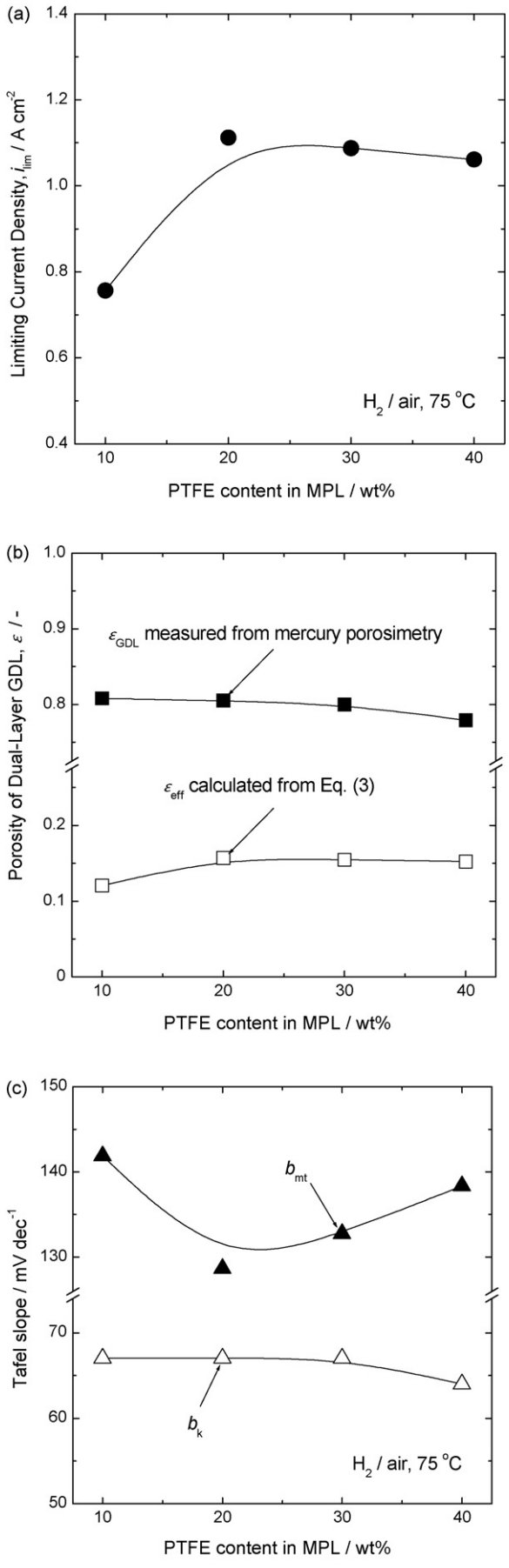

Fig. 5. Dependencies on the PTFE content in the MPL of (a) the limiting current density i_{lim}, (b) the effective porosity ε_{eff} (Eq. (3)) and the geometric porosity ε_{GDL} of dual-layer GDL, and (c) the kinetic Tafel slope b_k and the empirical Tafel slope b_{mt} (Eq. (2)). ε_{GDL} was estimated from the analyses of mercury intrusion data.

than 4.8, which implies the presence of a significant iR_2 drop. Given that the carbon-supported Pt catalyst is highly conductive, it appears that R_2 is mainly determined by the ionic resistance of thin ionomer films incorporated into the catalyst layer. The value of R_2 was determined from the $i - E_{iR_1\text{-corrected}}$ curves at $i_{air} > 400\,mA\,cm^{-2}$ by an iterative procedure, namely, the correct value of R_2 yielded $i_{O_2}/i_{air} \approx 4.8$. The polarization curves in Fig. 3(a) were corrected for the total ohmic losses (iR drop, where $R = R_1 + R_2$), and the results are presented for different PTFE loadings in Fig. 3(b). Table 2 lists the values of R_1 and R_2 estimated for different PTFE contents in the MPL, and as expected, both values remain almost constant, regardless of the PTFE content in the MPL.

Next, the iR-corrected polarization curves in Fig. 3(b) were reconstructed using the modified Tafel equation:

$$i_{kin} = \frac{i}{(1 - i/i_{lim})} = i'_o \exp\left(\frac{\eta_{iR\text{-corrected}}}{b_{mt}}\right) \quad (2)$$

where i_{lim} is the limiting current density, i_{kin} is the "kinetic" current density corrected for i_{lim}, $\eta_{iR\text{-corrected}}$ is the iR-corrected overpotential, and b_{mt} represents the empirical Tafel slope in the intermediate current densities. b_{mt} is distinguished from the kinetic Tafel slope b_k, in the low current densities, that characterizes the oxygen reduction kinetics in the absence of oxygen transport limitation in the catalyst layer [27].

The simulation study of Springer et al. [28] demonstrated that the limiting current density i_{lim} in low potential ranges is not affected by oxygen transport kinetics (or water saturation) in the catalyst layer, but it is exclusively controlled by oxygen concentration gradient which is established in the GDL. Therefore, it is reasonable to assume that when air is used as an oxidant, oxygen transport in the GDL is the only process responsible for the occurrence of limiting current phenomenon.

The value of i_{lim} was evaluated by an iterative procedure using Eq. (2), namely, the correct value of i_{lim} made the plot of $\eta_{iR\text{-corrected}}$ versus $\log i_{kin}$ a straight line. As an example, Fig. 4 demonstrates the iR-corrected polarization curves for 20 wt.% PTFE plotted in terms of (i) the measured current density i and (ii) the kinetic current density i_{kin}. Here, the value i_{kin} was calculated by taking i_{lim} as $1.11\,A\,cm^{-2}$. As shown in Fig. 4, Eq. (2) was valid for $i_{kin} > 1.0\,A\,cm^{-2}$.

The simulation analyses performed in the intermediate potential/current range [29–34] to study the effect of oxygen transport kinetics (or water saturation) in the catalyst layer on the polarization characteristics (current–potential relationship) of PEMFC indicated that the slope of the Tafel plot (logarithmic current versus cathodic overpotential) becomes two times larger than the kinetic Tafel slope measured in the activation control region. In other words, in the intermediate potential/current range the oxygen concentration polarization is significant in the catalyst layer and controls the performance of the fuel cell. As shown in

Fig. 4, when the measured current density was corrected for i_{lim}, the value of b_{mt} was found to be approximately two times higher than b_k, which is consistent with the theoretical prediction. This confirms that oxygen transport limitation in the catalyst layer is responsible for the observed increase of the Tafel slope in this study.

Fig. 5(a) shows the dependency of i_{lim} on the PTFE content in the MPL. It is seen that i_{lim} reaches a maximum value for 20 wt.% PTFE, indicating a minimum oxygen transport limitation (concentration polarization) in the GDL. The effective porosity ε_{eff} of the GDL, which represents the pore volume fraction available for oxygen transport, was calculated from i_{lim} using the following equation [28]:

$$\varepsilon_{eff} = \left[\frac{V_m l_{GDL} i_{lim}}{0.236 n F D_{ON} (T/273)^{0.823}}\right]^{1/1.5} \quad (3)$$

where V_m is the standard molar volume of gas (22,414 $cm^3\,mol^{-1}$), l_{GDL} the GDL thickness (ca. 0.05 cm), n the number of electrons transferred during oxygen reduction, F the Faraday constant, T the absolute temperature, and D_{ON} represents the oxygen/nitrogen binary diffusion coefficient (0.18 $cm^2\,s^{-1}$ [35]) at 1 atm and 273 K. The derivation of Eq. (3) is fully described in the paper of Springer et al. [28]. Fig. 5(b) presents the value of ε_{eff} as a function of PTFE content in the MPL, along with the GDL porosity, ε_{GDL}, determined experimentally from the mercury porosimetry (Fig. 1). The value of ε_{eff} is far lower than the GDL porosity, which means that most of pores in the GDL are occupied by liquid water, and only ca. 19% of the total porosity is available for oxygen diffusion in the GDL.

Next, b_{mt} was determined from the slope of a linear plot of $\eta_{iR\text{-corrected}}$ versus $\log i_{kin}$ in Fig. 4, and the results are presented in Fig. 5(c). The kinetic Tafel slope b_k was also evaluated from the *iR*-corrected polarization curves at $10\,mA\,cm^{-2} < i < 100\,mA\,cm^{-2}$ where we believe oxygen reduction is purely controlled by activation polarization in the absence of oxygen transport limitation. A minimum value of b_{mt} was observed for 20 wt.% PTFE, implying a minimum oxygen transport limitation (concentration polarization) in the catalyst layer.

In summary, the *ex situ* water permeation experiments indicated that the resistance to water flow through the double-layer GDL increases with PTFE loading in the MPL, which is attributed to an increased MPL hydrophobicity and a decreased MPL porosity. From the viewpoint of water management in a fuel cell, this result suggests that very high levels of PTFE loading in the MPL may impede water flow from the catalyst layer to the GDL, thus causing severe water flooding in the catalyst layer, whereas very low levels of PTFE loading may result in severe water flooding in the GDL. The electrochemical polarization studies demonstrated that the MPL loaded with 20 wt.% PTFE leads to the best fuel cell performance, showing the lowest b_{mt} (i.e., effective oxygen transport in the catalyst layer) and the highest i_{lim} (i.e., effective oxygen transport in the GDL). Consequently, it is conceivable that the optimized PTFE loading in the MPL results in a balanced water saturation in the catalyst layer and the GDL, thus improving oxygen transport kinetics during fuel cell operation.

Increasing the hydrophobicity of the catalyst layer may reduce the water saturation in the catalyst layer. On the other hand, an increased hydrophobicity of the catalyst layer results the GDL to become more susceptible to water flooding [18]. In this study, 20 wt.% PTFE loading in the MPL led to the best fuel cell performance; for a balanced water saturation the MPL should have higher percentage of PTFE than 20 wt.%, which will result in a higher hydrophobicity than that observed in this work.

4. Conclusion

The MPLs were prepared with different PTFE contents on the carbon-fiber substrates. The mercury porosimetry and water permeation experiments showed that PTFE increases the resistance to water flow through the GDL due to a decreased MPL porosity and an increased volume fraction of hydrophobic pores. When air was used as an oxidant, the MPL loaded with 20 wt.% PTFE led to the best fuel cell performance. The experimental polarization curves were analyzed to determine the concentration polarizations resulting from oxygen diffusion limitation in the GDL and the catalyst layer. The polarization analysis indicated that the optimized PTFE content reduces oxygen transport limitation in the catalyst layer as well as in the gas diffusion layer by controlling liquid water saturation in the MEA.

Acknowledgement

Financial support provided by FUJIFILM Manufacturing U.S.A., Inc. is acknowledged gratefully.

References

[1] F. Barbir, PEM Fuel Cells, Elsevier Academic Press, Burlington, 2005.
[2] M.S. Wilson, J.A. Valerio, S. Gottesfeld, Electrochim. Acta 40 (1995) 355–363.
[3] V.A. Paganin, E.A. Ticianelli, E.R. Gonzalez, J. Appl. Electrochem. 26 (1996) 297–304.
[4] L. Giorgi, E. Antolini, A. Pozio, E. Passalacqua, Electrochim. Acta 43 (1998) 3675–3680.
[5] F. Lufrano, E. Passalacqua, G. Squadrito, A. Patti, L. Giorgi, J. Appl. Electrochem. 29 (1999) 445–448.
[6] E. Passalacqua, G. Squadrito, F. Lufrano, A. Patti, L. Giorgi, J. Appl. Electrochem. 31 (2001) 449–454.
[7] E. Antolini, R.R. Passos, E.A. Ticianelli, J. Appl. Electrochem. 32 (2002) 383–388.
[8] Z. Qi, A. Kaufman, J. Power Sources 109 (2002) 38–46.
[9] C.-S. Kong, D.-Y. Kim, H.-K. Lee, Y.-G. Shul, T.-H. Lee, J. Power Sources 108 (2002) 185–191.
[10] J. Chen, T. Matsuura, M. Hori, J. Power Sources 131 (2004) 155–161.
[11] G. Lin, T.V. Nguyen, J. Electrochem. Soc. 152 (2005) A1942–A1948.
[12] Y. Song, Y. Wei, H. Xu, M. Williams, Y. Liu, L.J. Bonville, H.R. Kunz, J.M. Fenton, J. Power Sources 141 (2005) 250–257.
[13] S. Park, J.-W. Lee, B.N. Popov, J. Power Sources 163 (2006) 357–363.
[14] J.H. Nam, M. Kaviany, Int. J. Heat Mass Transfer 46 (2003) 4595–4611.
[15] A.Z. Weber, R.M. Darling, J. Newman, J. Electrochem. Soc. 151 (2004) A1715–A1727.

[16] U. Pasaogullari, C.-Y. Wang, Electrochim. Acta 49 (2004) 4359–4369.
[17] U. Pasaogullari, C.-Y. Wang, K.S. Chen, J. Electrochem. Soc. 152 (2005) A1574–A1582.
[18] A.Z. Weber, J. Newman, J. Electrochem. Soc. 152 (2005) A677–A688.
[19] M.V. Williams, E. Begg, L. Bonville, H.R. Kunz, J.M. Fenton, J. Electrochem. Soc. 151 (2004) A1173–A1180.
[20] G.-G. Park, Y.-J. Sohn, T.-H. Yang, Y.-G. Yoon, W.-Y. Lee, C.-S. Kim, J. Power Sources 131 (2004) 182–187.
[21] L.R. Jordan, A.K. Shukla, T. Behrsing, N.R. Avery, B.C. Muddle, M. Forsyth, J. Appl. Electrochem. 30 (2000) 641–646.
[22] E. Antolini, R.R. Passos, E.A. Ticianelli, J. Power Sources 109 (2002) 477–482.
[23] J. Bear, Dynamics of Fluids in Porous Media, American Elsevier Publishing Company, Inc., New York, 1972.
[24] J. Benziger, J. Nehlsen, D. Blackwell, T. Brennan, J. Itescu, J. Membr. Sci. 261 (2005) 98–106.
[25] M.E. Schrader, J. Phys. Chem. 79 (1975) 2508–2515.
[26] M.V. Williams, H.R. Kunz, J.M. Fenton, J. Electrochem. Soc. 152 (2005) A635–A644.
[27] A.J. Bard, L.R. Faulkner, Electrochemical Methods, second ed., John Wiley & Sons., New York, 2001.
[28] T.E. Springer, M.S. Wilson, S. Gottesfeld, J. Electrochem. Soc. 140 (1993) 3513–3526.
[29] J. Giner, C. Hunter, J. Electrochem. Soc. 116 (1969) 1124–1130.
[30] T.E. Springer, I.D. Raistrick, J. Electrochem. Soc. 135 (1989) 1594–1603.
[31] B.V. Tilak, S. Venkatesh, S.K. Rangarajan, J. Electrochem. Soc. 136 (1989) 1977–1982.
[32] I.D. Raistrick, Electrochim. Acta 25 (1990) 1579–1586.
[33] M.L. Perry, J. Newman, E.J. Cairns, J. Electrochem. Soc. 145 (1998) 5–15.
[34] F. Jaouen, G. Lindbergh, J. Electrochem. Soc. 150 (2003) A1699–A1710.
[35] F.P. Incropera, D.P. DeWitt, Fundamentals of Heat and Mass Transfer, fourth ed., John Wiley & Sons., New York, 1996.